Inorganic Chemistry Research

Article

Is the Superparamagnetic Iron Oxide Nanoparticle a Suitable Carrier for the Anticancer Drug Lenalidomide? A Quantum Chemical Approach

Monir Teymoori[a], Ali Morsali[a,b,*], Mohammad R. Bozorgmehr[a,b] and S. Ali Beyramabadi[a,b]

[a]*Department of Chemistry, Mashhad Branch, Islamic Azad University, Mashhad, Iran*
[b]*Research Center for Animal Development Applied Biology, Mashhad Branch, Islamic Azad University, Mashhad 917568, Iran*

Received: September 13, 2021; Accepted: October 21, 2021
Cite This: *Inorg. Chem. Res.* **2021**, *5*, 246-251. DOI: 10.22036/icr.2021.304579.1117

Abstract: The use of superparamagnetic iron oxide nanoparticles (SION) in targeted drug delivery has become widespread because they can be directed at cancerous tissue by applying an external magnetic field. In this work, we used quantum chemical calculations to investigate whether SIONs are suitable for the anticancer drug lenalidomide (LLM). For this purpose, using a suitable model for SION in aqueous solution, seven possible configurations of drug-carrier interaction were considered (SION/LLM1-7). The binding energies of optimized configurations were evaluated at M06-2X/6-31G(d,p). The most stable configurations (SION/LLM6 and SION/LLM7) occur when the drug is parallel to the nanoparticle ring. In these cases, the most and strongest hydrogen bonds are obtained. Large negative values of binding and solvation energies indicate high drug loading and acceptable solubility. Due to the essential role of hydrogen bonds in this drug delivery system, these bonds were studied in detail by quantum theory of atoms in molecules (QTAIM).

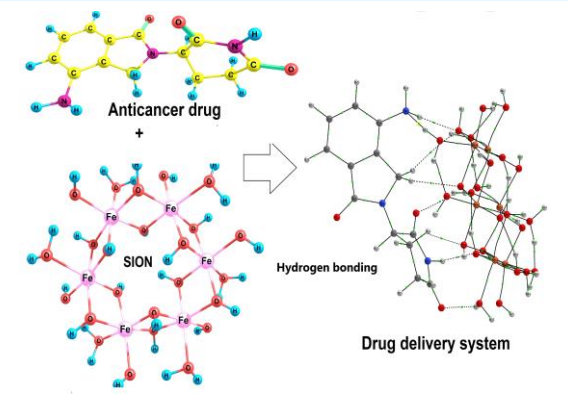

Keywords: Superparamagnetic iron oxide nanoparticles, Lenalidomide, DFT, AIM analysis, Drug delivery

1. INTRODUCTION

Cancer as one of the biggest threats to human health, accounts for a large part of scientific research. The use of nanomaterials for targeted drug delivery can greatly reduce the side effects of chemotherapy. In recent years, inorganic nanoparticles such as silica nanoparticles,[1,2] gold nanoparticles,[3,4] silver nanoparticles,[5] magnetic nanoparticles[6] and other inorganic nanoparticles[7-9] have been widely used.

Superparamagnetic nanoparticles such as iron oxide have the advantage that they can be directed to cancerous tissue using an external magnetic field.[10-12] The smaller size of these nanoparticles (20-40 nm) has the higher superparamagnetic properties.[13,14]

Many studies have been performed on two of the most well-known compositions of iron oxides (magnetite (Fe_3O_4) and maghemite (γ-Fe_2O_3))[15,16] in drug delivery systems.[17-19] These compounds have been used in the delivery of anti-cancer drugs such as cisplatin,[20] gemcitabine,[21] 5-flurouracil,[22] paclitaxel,[23] mitoxantrone,[24] doxorubicin[25] and temozolomide.[26]

One of the major problems in chemotherapy is the spread of the drug throughout the body and damage to healthy tissues.[27,28] Magnetic nanoparticle-based drug delivery systems significantly reduce side effects by targeted drug delivery.[29,30] The drug at the destination can be released by techniques such as changes in temperature and PH.[31-33] Renal excretion is the best way to remove superparamagnetic iron oxide nanoparticles from the body because the possibility of producing reactive oxygen species is reduced and intracellular catabolism is minimal.[34] Mahmoudi et al.[35] conducted a comprehensive study on these nanoparticles toxicity and concluded that superparamagnetic iron oxide nanoparticles are compatible with kidney cells but are toxic to brain cells. Considering the dose of nanoparticles used in targeted drug delivery, there is no potential risk to other organs.

1-oxo-2-(2,6-dioxopiperidin-3-yl)-4-aminoisoindoline or lenalidomide is an analogue of thalidomide and an anticancer drug. It is prescribed to treat a variety of cancers, including multiple myeloma (MM),[36] prostate cancer,[37] myelodysplastic syndromes,[38] pancreatic cancer,[39] ovarian cancer,[40] chronic lymphocytic leukemia[41] and non-Hodgkin's lymphoma.[42]

To design new drug delivery systems, a better understanding of the mechanism of drug-carrier interaction is essential.[43-46] Computational quantum chemistry is a good tool for studying molecular interactions in drug delivery systems.[47-49] In this work, using an applied quantum chemical model for iron oxide nanoparticles in aqueous solution,[50-53] we investigated the interaction of these superparamagnetic nanoparticles with the anti-cancer drug lenalidomide. The results can be useful for experimental scientists in choosing the right nanocarrier for lenalidomide.

2. COMPUTATIONAL METHOD

All optimizations were performed by the GAUSSIAN 09 software[54] at M06-2X density functional level of theory with 6-31G(d,p) basis set for all atoms except Fe, for which LANL2DZ basis set[55] with effective core potential (ECP) functions was employed. M06-2X functional[56,57] was chosen because it considers dispersion corrections[58] in noncovalent interactions. Frequency calculations were done in order to consider the thermal energy correction. All molecular structures were checked to have no imaginary frequency.

In biological systems, solvent plays an important role in the structure and energy of species. These effects were applied by polarized continuum model (PCM).[59,60] In this method, the molecular free energy is calculated by the following equation:

$$G_{sol} = G_{es} + G_{dr} + G_{cav} \quad (1)$$

where G_{es}, G_{dr} and G_{cav} represent the electrostatic, dispersion-repulsion and cavitation free energies, respectively. Aqueous solution was considered, because H_2O is the major solvent in the body.

The gap of energy (E_g), global hardness (η) and electrophilicity index (ω) (quantum molecular descriptors) may be calculated (Eqs. (1)-(3)) by HOMO and LUMO energies. The stability of the structures was also examined by these descriptors.[61,62]

$$E_g = E_{LUMO} - E_{HOMO} \quad (2)$$

$$\eta = \frac{I - A}{2} \quad (3)$$

$$\omega = \frac{(I + A)^2}{8\eta} \quad (4)$$

where $I = -E_{HOMO}$ (ionization potential) and $A = -E_{LUMO}$ (electron affinity).

Examination of the structures obtained from quantum chemical calculations showed that hydrogen bonds play an important role in this drug delivery system, which requires a more detailed study with quantum theory of atoms in molecules (QTAIM).[63] This theory uses the topological analysis of electron density ($\rho(r)$, Laplacian of electron density ($\nabla^2\rho$), potential energy density (V_b), kinetic energy density (G_b) and total energy density (H_b) at a bond critical point (BCP). AIMAII software[64] was used to calculate these parameters.

3. RESULTS AND DISCUSSION

Binding and solvation energies

Experimental evidence shows that superparamagnetic iron oxide nanoparticles (SION) in aqueous solution can be modelled with a ring of six octahedra connected by twelve OH groups plus six surface OH and H_2O groups ($Fe_6(OH)_{18}(H_2O)_6$).[50] Figure 1 shows the optimized structure of SION and lenalidomide (with NH_2, NH and CO functional groups). Lenalidomide (LLM) can form hydrogen bonds with SION surface OH and H_2O groups through its functional groups. The drug (LLM) can approach the nanocarrier (SION) from different directions, resulting in seven main configurations (SION/LLM1-7) shown in Figures 2 and 3.

One of the important parameters that shows the strength of the overall interaction between the drug and the nanocarrier and can also be a measure of drug loading[65,66] is the binding energy (ΔE_{bind})

$$\Delta E_{bind} = E_{SION/LLM1-7} - (E_{SION} - E_{LLM}) \quad (5)$$

where $E_{SION/LLM1-7}$, E_{SION} and E_{LLM} are the energies of SION/LLM1-7, SION and LLM, respectively. The binding and absolute energies in aqueous solution were represented in Table 1.

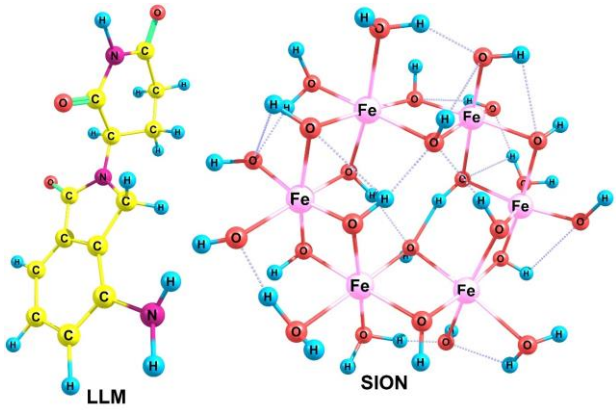

Figure 1. Optimized structures of SION and LLM.

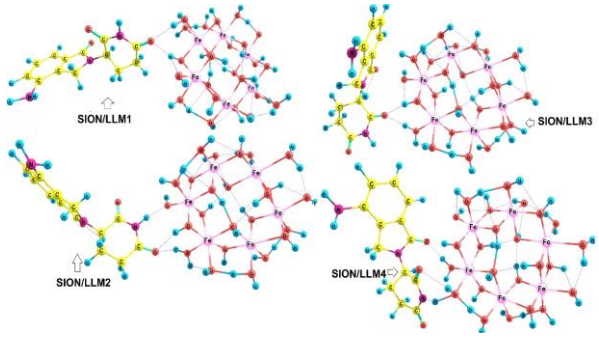

Figure 2. Optimized structures of SION/LLM1-4.

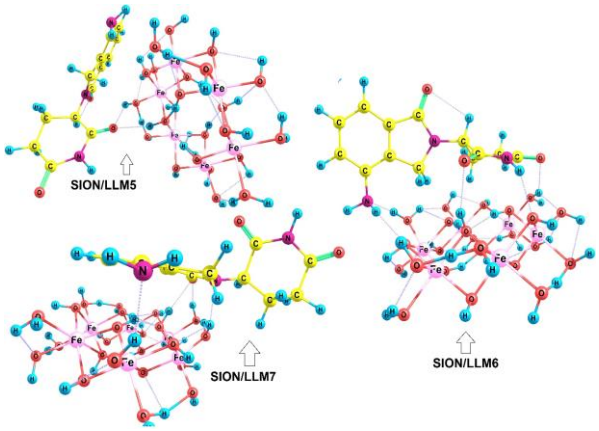

Figure 3. Optimized structures of SION/LLM5-7.

Table 1. Absolute energies (E: Hartree), binding energies (ΔE_{bind}: kJ mol^{-1}) and solvation energies (ΔE_{solv}: kJ mol^{-1}) of SION/LLM1-7 in gas (E_g) and solution (E_s) phases

Species	E_s	ΔE_{bind}	E_g	ΔE_{solv}	$\Delta E_{R,i}$	$e^{-\frac{\Delta E_{R,i}}{kT}}$	P_i
SION	-2562.872329	-	-	-	-	-	-
LLM	-892.612413	-	-	-	-	-	-
SION/LM1	-3455.488878	-10.9	-3455.413516	-197.9	75.1	6.9E-14	6.9E-14
SION/LM2	-3455.494753	-26.3	-3455.419912	-196.5	59.7	3.5E-11	3.5E-11
SION/LM3	-3455.497522	-33.6	-3455.420258	-202.9	52.4	6.6E-10	6.6E-10
SION/LM4	-3455.498817	-37.0	-3455.418739	-210.2	49.0	2.6E-09	2.6E-09
SION/LM5	-3455.497938	-34.6	-3455.427554	-184.8	51.3	1.0E-09	1.0E-09
SION/LM6	-3455.517475	-85.9	-3455.443288	-194.8	0.0	1.0E+00	1.0E+00
SION/LM7	-3455.502795	-47.4	-3455.425641	-202.6	38.5	1.8E-07	1.8E-07

SION/LLM6 and SION/LLM7 configurations have the most negative binding energies (strongest interactions), respectively, in which the drug is placed parallel to the nanoparticle ring. A quick look at Figures 2 and 3 shows that the more hydrogen bonds are formed, the more stable the structure. For this reason, in the next section, these hydrogen bonds will be examined in more detail.

To evaluate the average binding energy ($\overline{\Delta E}$), it is necessary to calculate the thermodynamic probability (P_i) from the following equations:

$$\overline{\Delta E} = \sum P_i E_i \qquad (6)$$

$$P_i = \frac{e^{-\frac{\Delta E_{R,i}}{kT}}}{\sum e^{-\frac{\Delta E_{R,i}}{kT}}} \qquad (7)$$

where $\Delta E_{R,i} = E_i - E_6$, T and k are relative binding energy (Table 2), temperature and Boltzmann constant, respectively. E_6 is the energy of SION/LLM6 configuration (the most stable configuration).[52] The values in Table 1 clearly show that the SION/LLM6 configuration plays a major role in determining the average binding energy. High average binding energy ($\overline{\Delta E}$ = -85.9 kJ mol^{-1}) indicates that iron oxide nanoparticle is a good carrier for LLM and drug loading is predicted to be appropriate.

The solvation energies (ΔE_{solv}) can be calculated using the following equation:

$$\Delta E_{solv} = E_{sol} - E_{gas} \qquad (8)$$

where E_{gas} and E_{gas} show the total energies in the gas and solution phases. Table 1 also presents the absolute energies in gas phase. The large negative values of ΔE_{solv} indicate that the solvation process is spontaneous. One of the advantages of LLM is that it has functional groups such as NH_2, NH and CO that can form hydrogen bonds with solvent molecules (H_2O) and OH and H_2O groups of iron oxide nanoparticles to increase solubility.

QTAIM analysis and quantum molecular descriptors

In this drug delivery system, hydrogen bonds play an important role in binding and solvation energies. These intermolecular interactions can be studied in more detail by QTAIM. The values of $\rho(r)$, $\nabla^2\rho(r)$, H_b, G_b, V_b and $-G_b/V_b$ for SION/LLM1-7 were presented in Table 2. This

Table 2. Topological parameters (a.u.) and E_{HB} (kJ mol^{-1}) of SION/LLM1-7.

Atoms	$\rho(r)$	$\nabla^2\rho(r)$	G_b	V_b	H_b	$-G_b/V_b$	E_{HB}
SION/LLM 6							
N6-H62	0.0586	0.1064	0.0364	-0.0462	-0.0098	0.7878	-60.6
H32 - O43	0.0247	0.0751	0.0199	-0.0211	-0.0011	0.9459	-27.6
O2-H90	0.0153	0.0483	0.0122	-0.0123	-0.0001	0.9890	-16.2
H27 - O35	0.0220	0.0665	0.0174	-0.0182	-0.0008	0.9563	-23.9
O3-H63	0.0134	0.0447	0.0111	-0.0109	0.0001	1.0110	-14.3
H23 - O43	0.0047	0.0182	0.0036	-0.0027	0.0009	1.3499	-3.5
H24 - O50	0.0114	0.0366	0.0087	-0.0083	0.0004	1.0514	-10.9
H22 - O45	0.0111	0.0392	0.0090	-0.0082	0.0008	1.0964	-10.8
SION/LLM 7							
O1-H80	0.0118	0.0474	0.0107	-0.0096	0.0011	1.1167	-12.6
O1-H83	0.0166	0.0500	0.0128	-0.0130	-0.0003	0.9789	-17.1
N4-H54	0.0249	0.0689	0.0181	-0.0189	-0.0009	0.9549	-24.8
N6-H78	0.0232	0.0603	0.0160	-0.0169	-0.0009	0.9458	-22.2
H29 - O59	0.0039	0.0162	0.0032	-0.0024	0.0008	1.3354	-3.2
H30 - O37	0.0044	0.0171	0.0033	-0.0024	0.0009	1.3924	-3.1
H28 - O34	0.0019	0.0080	0.0015	-0.0009	0.0005	1.5956	-1.2
H24-O49	0.0087	0.0341	0.0073	-0.0061	0.0012	1.2054	-7.9
SION/LLM 4							
O1-H67	0.0315	0.1089	0.0207	-0.0212	-0.0005	0.9768	-27.8
H27-O70	0.0529	0.1418	0.0296	-0.0338	-0.0042	0.8764	-44.4
O2 -87	0.0103	0.0413	0.0093	-0.0083	0.0010	1.1214	-10.9
O1-H87	0.0098	0.0329	0.0079	-0.0075	0.0004	1.0483	-9.8
H28-O71	0.0051	0.0196	0.0040	-0.0031	0.0009	1.2798	-4.1
SION/LLM 5							
O2-H90	0.0156	0.0549	0.0183	-0.0229	-0.0046	0.7991	-30.1
O2-H77	0.0203	0.0639	0.0196	-0.0272	-0.0076	0.7202	-35.7
N4-H77	0.0104	0.0349	0.0080	-0.0073	0.0007	1.1006	-9.5
H32-O61	0.0054	0.0231	0.0048	-0.0038	0.0010	1.2523	-5.0
H31-O71	0.0092	0.0342	0.0076	-0.0067	0.0009	1.1392	-8.8
H23-O43	0.0118	0.0395	0.0093	-0.0087	0.0006	1.0701	-11.4
SION/LLM 3							
O2-H67	0.0293	0.0929	0.0233	-0.0234	-0.0001	0.9966	-30.7
O2-H87	0.0227	0.0702	0.0180	-0.0185	-0.0005	0.9736	-24.3
O2-O71	0.0225	0.0768	0.0190	-0.0127	0.0062	1.4885	-16.7
SION/LLM 2							
O2-H67	0.0289	0.0989	0.0228	-0.0228	-0.0001	0.9972	-30.0
O3-H87	0.0165	0.0576	0.0141	-0.0138	0.0003	1.0219	-18.1
O3-H67	0.0083	0.0295	0.0071	-0.0068	0.0003	1.0430	-8.9
SION/LLM 1							
O3-H87	0.0271	0.0849	0.0216	-0.0220	-0.0004	0.9832	-28.8
O3-H67	0.0219	0.0813	0.0194	-0.0125	0.0069	1.5543	-16.4

table also reports the hydrogen bond energies (E_{HB} = $V_b/2$).[67] Figures 4 and 5 shows the molecular graphs of these structures.

We first examine the most stable configuration (SION/LLM6). N6··· H62 interaction with E_{HB} = -60.6 kJ mol^{-1} is the strongest interaction in all configurations and is classified as medium hydrogen bonds ($\nabla^2\rho > 0$, $H_b < 0$, $0.5 < -G_b/V_b < 1$).[68] In this configuration, where the LLM drug is parallel to the nanocarrier ring, there are four other medium hydrogen bonds, although their hydrogen bond energies are less than the previous case (H32··· O43, H90··· O2 and H27··· O35) and a weak hydrogen bond (H63··· O3) with ($\nabla^2\rho > 0$, $H_b > 0$ and $-G_b/V_b > 1$[68]. Interactions with less hydrogen bond energy than previous cases can be classified as pseudo hydrogen bonds (CH··· O). For this configuration, three of these types of interactions are listed in Table 2 (CH23··· O43, CH24··· O50 and CH22··· O45).

SION/LLM7 configuration, as the second most stable structure, is almost parallel to the nanoparticle ring but produces weaker hydrogen bonds than the previous configuration. This configuration has three medium hydrogen bonds (H83··· O1, H54··· N4 and H78··· N6) with hydrogen bond energies less than 25 kJ mol^{-1} and a weak hydrogen bond (H83··· O1) with E_{HB} = -12.6 kJ mol^{-1}. The other four interactions with hydrogen bond energies less than 8 kJ mol^{-1} are pseudo hydrogen bonds.

SION/LLM5, SION/LLM4 and SION/LLM3 have almost the same stability. All three configurations have two medium hydrogen bonds (Table 2). In these configurations, there are three, two, and one weak hydrogen bond, respectively. Each of SION/ configurations LLM5 and SION/LLM4 configurations has a pseudo hydrogen bond. The most unstable configurations are SION/LLM1 and SION/LLM2 configurations, respectively. Both configurations have a medium hydrogen bond (Table 2).

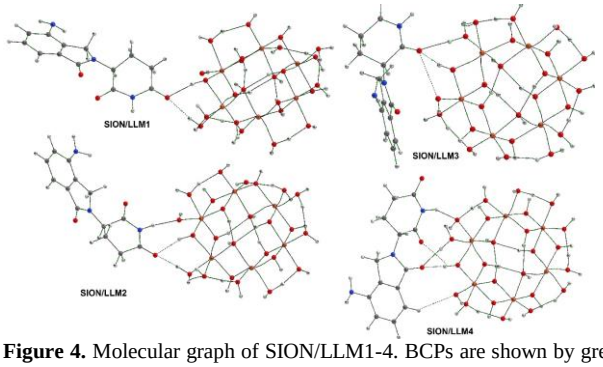

Figure 4. Molecular graph of SION/LLM1-4. BCPs are shown by green spheres.

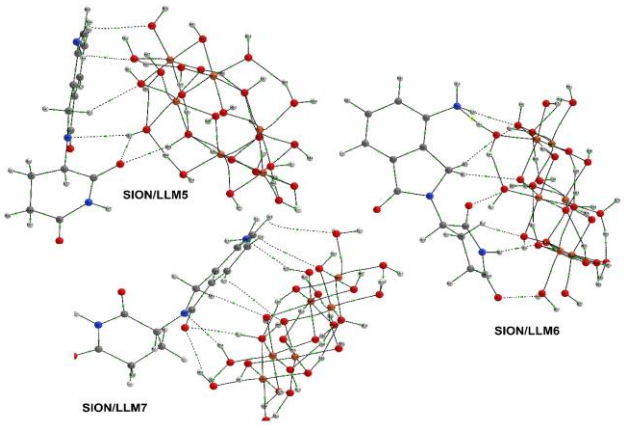

Figure 5. Molecular graph of SION/LLM5-7.

The values of ω and η (quantum molecular descriptors), as well as E_g (band gap between LUMO and HOMO) for LLM, SION and SION/LLM1-7 were presented in Table 3. LLM with large values of η (5.58 eV) and E_g (5.58 eV) is the stable structure. As the nanocarrier is functionalized by LLM, η and E_g are significantly reduced, therefore the reactivity of the drug is increased.

A sudden change in band gap (E_g) can be the basis for building a sensor to detect LLM because the electrical conductivity is proportional to exp($-E_g/2kT$). Therefore, iron oxide nanoparticles can be used both in carrying LLM and in making sensors for it. The ù value of LLM (1.82 eV) increases as a result of functionalization, which indicates that in this drug delivery system, LLM is an electron acceptor.

Table 3 also shows the recovery times (ô), which is an important parameter for drug delivery systems.[69,70] ô for the LLM anticancer drug desorption from the SION surface may be evaluated using the following equation:

$$\tau = \nu^{-1} e^{\frac{\Delta E_{bind}}{kT}} \qquad (9)$$

where ν is the attempt frequency. By applying a UV of 10^{16} Hz (≈ 30 nm: approximately proportional to the average SION length) at 298 K for í, the ô values in Table 3 were obtained.

Short recovery times (0.12 s for the most stable configuration) also indicate that SION is a suitable nanocarrier for LLM anticancer drug.

Table 3. Quantum molecular descriptors (eV) and recovery times (τ) of calculated structures

Species	E_{HOMO}	E_{LUMO}	Eg	η	ω	τ (s)
LLM	-7.20	-0.02	7.18	3.59	1.82	-
SION	-7.79	-3.85	3.94	1.97	8.59	-
SION/LLM1	-7.20	-3.76	3.44	1.72	8.73	8.0E-15
SION/LLM2	-7.20	-3.93	3.27	1.63	9.47	4.0E-12
SION/LLM3	-7.37	-3.71	3.66	1.83	8.40	7.6E-11
SION/LLM4	-7.25	-3.72	3.54	1.77	8.52	3.0E-10
SION/LLM5	-7.45	-3.88	3.57	1.79	8.97	1.2E-10
SION/LLM6	-7.72	-3.82	3.90	1.95	8.52	1.2E-01
SION/LLM7	-7.56	-3.66	3.90	1.95	8.06	2.0E-08

4. CONCLUSION

Due to the increasing use of superparamagnetic iron oxide nanoparticles (SION) in drug delivery systems, the effectiveness of these nanoparticles in carrying the anti-cancer drug lenalidomide (LLM) was evaluated using quantum chemical methods. Seven possible configurations of SION ($Fe_6(OH)_{18}(H_2O)_6$ ring cluster) were optimized alongside the LLM drug (SION/LLM1-7) at M06-2X/6-31G(d,p) in aqueous solution. The most stable configuration (SION/LLM6) has the largest contribution in determining the average binding energy and its large negative value indicates high drug loading.

Calculated values of solvation energies indicate that this process is spontaneous due to the formation of hydrogen bonds. These bonds are also the main cause of high adsorption energy and therefore were studied in more detail by quantum theory of atoms in molecules (QTAIM).

In SION/LLM6 configuration (the most stable configuration), where LLM is placed parallel to the nanoparticle ring, more and stronger hydrogen bonds are formed. Alteration of drug band gap due to adsorption on nanoparticles indicates that this nanocarrier can be also used in the manufacture of sensors to detect LLM. Due to high adsorption energy (high drug loading), acceptable solubility and the presence of hydrogen bonds, SIONs are expected to be a suitable nanocarrier for LLM.

CONFLICTS OF INTEREST

There are no conflicts to declare.

AUTHOR INFORMATION

Corresponding Author(s)

Ali Morsali: Email: almorsali@yahoo.com; morsali@mshdiau.ac.ir, *ORCID*: 0000-0002-8569-2442.

Author(s)

Monir Teymoori, Mohammad R. Bozorgmehr, S. Ali Beyramabadi

ACKNOWLEDGEMENTS

We thank the Research Center for Animal Development Applied Biology for allocation of computer time. This research did not receive any specific grant from funding agencies in the public, commercial or not-for-profit sectors.

REFERENCES

1. Y. Li, N. Li, W. Pan, Z. Yu, L. Yang, B. Tang, *ACS Appl. Mater. Interfaces*, **2017**, *9*, 2123-2129.
2. F. Naghavi, A. Morsali, M. R. Bozorgmehr, *J. Mol. Liq.*, **2019**, *282*, 392-400.
3. D. M. Connor, A. -M. Broome, *Adv. Cancer Res.*, **2018**, *139*, 163-184.
4. K. Bansal, N. Devi, M. Aqdas, R. K. Sharma, J. N. Agrewala, O. Katare, *J. Mol. Liq.*, **2021**, *328*, 115385.
5. L. Wei, J. Lu, H. Xu, A. Patel, Z. -S. Chen, G. Chen, *Drug Discov. Today*, **2015**, *20*, 595-601.
6. A. Taheri-Kafrani, H. Shirzadfar, E. Tavassoli-Kafrani, Nano-and Microscale Drug Delivery Systems, Elsevier, **2017**, p. 75-94.
7. D. C. Luther, R. Huang, T. Jeon, X. Zhang, Y. -W. Lee, H. Nagaraj, V. Rotello, *Adv. Drug Deliv. Rev.*, **2020**, *156*, 188-213.
8. H. R. Mardani, M. Forouzani, S. Geraeeli Moradi, *Inorg. Chem. Res.*, **2021**, *5*, 207-214.
9. S. Khani, M. Montazerzohori, R. Naghiha, S. Joohari, *Inorg. Chem. Res.*, **2020**, *4*, 279-294.
10. S. Mornet, S. Vasseur, F. Grasset, E. Duguet, *J. Mater. Chem.*, **2004**, *14*, 2161-2175.
11. A. Ito, M. Shinkai, H. Honda, T. Kobayashi, *J. Biosci. Bioeng.*, **2005**, *100*, 1-11.
12. A. Singh, F. Dilnawaz, S. Mewar, U. Sharma, N. Jagannathan, S. K. Sahoo, *ACS Appl. Mater. Interfaces*, **2011**, *3*, 842-856.
13. R. Roohi, H. Emdad, K. Jafarpur, *J. Test. Eval.*, **2019**, *47*, 681-703.
14. K. Jain, *BMC Medicine*, **2010**, *8*, 83.
15. L. Douziech-Eyrolles, H. Marchais, K. Herve, E. Munnier, M. Souce, C. Linassier, P. Dubois, I. Chourpa, *Int. J. Nanomedicine*, **2007**, *2*, 541.
16. M. Mahmoudi, S. Sant, B. Wang, S. Laurent, T. Sen, *Adv. Drug Deliv. Rev.*, **2011**, *63*, 24-46.
17. R. Tietze, S. Lyer, S. Dürr, T. Struffert, T. Engelhorn, M. Schwarz, E. Eckert, T. Göen, S. Vasylyev, W. Peukert, *Nanomedicine*, **2013**, *9*, 961-971.
18. C. Fang, M. Zhang, *J. Mater. Chem.*, **2009**, *19*, 6258-6266.
19. K. T. Al-Jamal, J. Bai, J. T. -W. Wang, A. Protti, P. Southern, L. Bogart, H. Heidari, X. Li, A. Cakebread, D. Asker, *Nano Lett.*, **2016**, *16*, 5652-5660.
20. P. A. Ma, H. Xiao, C. Yu, J. Liu, Z. Cheng, H. Song, X. Zhang, C. Li, J. Wang, Z. Gu, *Nano Lett.*, **2017**, *17*, 928-937.
21. D. H. Kim, Y. Guo, Z. Zhang, D. Procissi, J. Nicolai, R. A. Omary, A. C. Larson, *Adv. Healthc. Mater.*, **2014**, *3*, 714-724.
22. J. L. Arias, V. Gallardo, M. A. Ruiz, Á. V. Delgado, *Eur. J. Pharm. Biopharm.*, **2008**, *69*, 54-63.
23. Y. C. Chen, W. F. Lee, H. H. Tsai, W. Y. Hsieh, *J. Biomed. Mater. Res. A*, **2012**, *100*, 1279-1292.
24. M. G. Krukemeyer, V. Krenn, M. Jakobs, W. Wagner, *J. Surg. Res.*, **2012**, *175*, 35-43.
25. K. Zhu, Z. Deng, G. Liu, J. Hu, S. Liu, *Macromolecules*, **2017**, *50*, 1113-1125.
26. U. K. Sukumar, R. J. Bose, M. Malhotra, H. A. Babikir, R. Afjei, E. Robinson, Y. Zeng, E. Chang, F. Habte, R. Sinclair, *Biomaterials*, **2019**, *218*, 119342.

27. G. D. Pennock, W. S. Dalton, W. R. Roeske, C. P. Appleton, K. Mosley, P. Plezia, T. P. Miller, S. E. Salmon, *J. Natl. Cancer Inst*., **1991**, *83*, 105-110.
28. C. Lindley, J. S. McCune, T. E. Thomason, D. Lauder, A. Sauls, S. Adkins, W. T. Sawyer, *Cancer Pract.*, **1999**, *7*, 59-65.
29. M. -Y. Hua, H. -L. Liu, H. -W. Yang, P. -Y. Chen, R. -Y. Tsai, C. -Y. Huang, I. -C. Tseng, L. -A. Lyu, C. -C. Ma, H. -J. Tang, *Biomaterials*, **2011**, *32*, 516-527.
30. H. Kempe, M. Kempe, *Biomaterials*, **2010**, *31*, 9499-9510.
31. J. Dobson, *Drug Dev. Res*., **2006**, *67*, 55-60.
32. H. Bi, X. Han, *Chem. Phys. Lett.*, **2018**, *706*, 455-460.
33. M. Namdeo, S. Saxena, R. Tankhiwale, M. Bajpai, Y. Mohan, S. Bajpai, *J. Nanosci. Nanotechno*l., **2008**, *8*, 3247-3271.
34. S. A. Wahajuddin, *Int. J. Nanomedicine*, **2012**, *7*, 3445-3471.
35. M. Mahmoudi, H. Hofmann, B. Rothen-Rutishauser, A. Petri-Fink, *Chem. Rev.*, **2011**, *112*, 2323-2338.
36. T. Hideshima, P. G. Richardson, K. C. Anderson, *Expert Opin. Investig. Drugs*, **2006**, *15*, 171-179.
37. L. Sundaresan, P. Kumar, S. Chatterjee, *Future Oncol*., **2018**, *14*, 2383-2401.
38. M. Stahl, A. M. Zeidan, *Cancer*, **2017**, *123*, 1703-1713.
39. G. J. Ullenhag, F. Mozaffari, M. Broberg, H. Mellstedt, M. Liljefors, *PloS One*, **2017**, *12*, e0169736.
40. C. B. Tempfer, B. Schultheis, Z. Hilal, A. Dogan, G. A. Rezniczek, *Oncol. Lett*., **2017**, *14*, 3327-3336.
41. A. P. Kater, S. H. Tonino, A. Egle, A. G. Ramsay, *Blood*, **2014**, *124*, 2184-2189.
42. S. Yamshon, P. J. Christos, M. Demetres, H. Hammad, J. P. Leonard, *J. Ruan, Blood Adv.*, **2018**, *2*, 1429-1438.
43. F. Naghavi, A. Morsali, M. R. Bozorgmehr, S. A. Beyramabadi, *J. Mol. Liq.*, **2020**, *310*, 113155.
44. M. Nasrabadi, S. A. Beyramabadi, A. Morsali, *Int. J. Biol. Macromol.*, **2020**, *147*, 534-536.
45. M. Rahbar, A. Morsali, M. R. Bozorgmehr, S. A. Beyrmabadi, *J. Mol. Liq.*, **2020**, *302*, 112495.
46. M. Najafi, A. Morsali, M. R. Bozorgmehr, *Struct. Chem*., **2018**, *30*, 715-726.
47. M. Nasrabadi, A. Morsali, S. A. Beyramabadi, *Int. J. Biol. Macromol.*, **2020**, *165*, 1229-1240.
48. S. Moghimi, A. Morsali, M. M. Heravi, S. A. Beyramabadi, *Inorg. Chem. Res.*, **2021**, *5*, 120-131.
49. M. Lotfi, A. Morsali, M. R. Bozorgmehr, *Appl. Surf. Sci.*, **2018**, *462*, 720-729.
50. L. Jayarathne, W. J. Ng, A. Bandara, M. Vitanage, C. Dissanayake, R. Weerasooriya, *Colloids Surf. A*, **2012**, *403*, 96-102.
51. H. Lari, A. Morsali, M. M. Heravi, *Z. Phys. Chem*., **2018**, *232*, 579-592.
52. A. Rezaei, A. Morsali, M. R. Bozorgmehr, M. Nasrabadi, *J. Mol. Liq.*, **2021**, *340*, 117182.
53. Z. Shabani, A. Morsali, M. R. Bozorgmehr, S. A. Beyramabadi, *Chem. Phys. Lett.*, **2019**, *719*, 12-21.
54. M. Frisch, G. Trucks, H. Schlegel, G. Scuseria, M. Robb, J. Cheeseman, G. Scalmani, V. Barone, B. Mennucci, G. Petersson, Gaussian Inc., Wallingford, **2009**,
55. P. J. Hay, W. R. Wadt, *J. Chem. Phys.*, **1985**, *82*, 299-310.
56. Y. Zhao, N. E. Schultz, D. G. Truhlar, *J. Chem. Theory Comput.*, **2006**, *2*, 364-382.
57. Y. Zhao, D. G. Truhlar, *J. Chem. Phys.*, **2006**, *125*, 194101.
58. Y. Zhao, D. G. Truhlar, *Theor. Chem. Acc.*, **2008**, *120*, 215-241.
59. J. Tomasi, M. Persico, *Chem. Rev.*, **1994**, *94*, 2027-2094.
60. R. Cammi, J. Tomasi, *J. Comput. Chem.*, **1995**, *16*, 1449-1458.
61. M. Kamel, H. Raissi, A. Morsali, *J. Mol. Liq.*, **2017**, *248*, 490-500.
62. R. Khorram, H. Raissi, A. Morsali, *J. Mol. Liq.*, **2017**, *240*, 87-97.
63. R. F. Bader, *Chem. Rev.*, **1991**, *91*, 893-928.
64. T. A. Keith, TK Gristmill Software, Overland Park KS, USA, **2013**,
65. P. Geetha, A. J. Sivaram, R. Jayakumar, C. G. Mohan, *Carbohydr. Polym.*, **2016**, *142*, 240-249.
66. S. -H. Lin, W. Cui, G. -L. Wang, S. Meng, Y. -C. Liu, H. -W. Jin, L. -R. Zhang, Y. Xie, *Drug Des. Devel. Ther*., **2016**, *10*, 2973-2987.
67. E. Espinosa, M. Souhassou, H. Lachekar, C. Lecomte, *Acta Crystallogr. Sect. B: Struct. Sci.*, **1999**, *55*, 563-572.
68. I. Rozas, I. Alkorta, J. Elguero, *J. Am. Chem. Soc.*, **2000**, *122*, 11154-11161.
69. N. T. Si, N. T. A. Nhung, T. Q. Bui, M. T. Nguyen, P. V. Nhat, *RSC Adv.*, **2021**, *11*, 16619-16632.
70. T. Ma, C. Jin, S. A. Aslanzadeh, *Int. J. Quantum Chem.*, **2020**, *120*, e26407.